Inorg. Chem. **2007**, *46*, 5179–5187

Indium Hydroxides, Oxyhydroxides, and Oxides Nanocrystals Series

Zhongbin Zhuang, Qing Peng,* Junfeng Liu, Xun Wang, and Yadong Li*

Department of Chemistry, Tsinghua University, Beijing, 100084, Peoples Republic of China

Received October 18, 2006

Indium hydroxides, oxyhydroxides, and oxides are important n-type semiconductors and have wide applications in material fields. In this Article, a series of $In(OH)_3$ and InOOH nanocrystals with different structures and morphologies, such as nanocubes, nanorods, multipods, and nanoparticles, have been synthesized selectively through a liquid-phase reaction, by adjusting the alkalinity and polarity of the solvent. It is found that InOOH multipods are in the orthorhombic phase and their arms grow along nonequivalent faces. Cubic and hexagonal In_2O_3 can be obtained from $In(OH)_3$ and InOOH, respectively, while size and morphology can be maintained to a certain extent. Gas sensors were fabricated by using In_2O_3, and a device based on the multipods shows the best responses to ethanol vapor. XRD, TEM, HRTEM, SEM, and SAED have been used to characterize these nanocrystals. This work provides a preliminary investigation into the structural-based gas-sensing properties of these nanocrystals.

Introduction

Controlled synthesis of nanocrystals with specific structures and research into their structural-based properties are important subjects in nanoscience.[1−3] At the nanometer scale, the size and shape of nanocrystals become significant factors to their properties because they relate to the density of electronic states.[4−6] Coupled nanocrystals can form advanced structures, such as star-shaped 3D multipods. These structures can be determined as novel single-electron transistors and fabricate multiple terminals directly.[7−9] In the past decade, the thermolysis approach and the hot-injection method have shown good ability to control the size and shape of nanocrystals, and many high-quality colloidal nanocrystals have been obtained.[2,10,11] However, up to now, controllable synthesis of nanocrystals with desired structure and morphology is still a challenge for scientists.

Indium hydroxides, oxyhydroxides, and oxides are a series of important semiconductor materials, which have gained much more attention in past decade. Cubic $In(OH)_3$, orthorhombic InOOH, and cubic and hexagonal In_2O_3 are their common phases.[12] $In(OH)_3$ is a wide-gap semiconductor with $E_g = 5.15$ eV and has applications as a photocatalyst, and so forth.[13] InOOH ($E_g = 3.5$ eV) is a typical wide-gap

* To whom correspondence should be addressed. E-mail: pengqing@mail.tsinghua.edu.cn (Q.P.), ydli@mail.tsinghua.edu.cn (Y.L.).

(1) Cushing, B. L.; Kolesnichenko, V. L.; O'Connor, C. J. *Chem. Rev.* **2004**, *104*, 2893.
(2) (a) Peng, X. G. *Adv. Mater.* **2003**, *15*, 459. (b) Yin, Y. D.; Alivisatos, A. P. *Nature* **2005**, *437*, 664. (c) Jun, Y. W.; Choi, J. S.; Cheon, J. W. *Angew. Chem., Int. Ed.* **2006**, *45*, 3414.
(3) (a) Xia, Y.; Gates, B.; Yin, Y.; Lu, Y. *Adv. Mater.* **2000**, *12*, 693. (b) Xia, Y.; Yang, P.; Sun, Y.; Wu, Y.; Mayers, B.; Gates, B.; Yin, Y.; Kim, F.; Yan, H. *Adv. Mater.* **2003**, *15*, 353.
(4) (a) Alivisatos, A. P. *Science* **1996**, *271*, 933. (b) El-Sayed, M. A. *Acc. Chem. Res.* **2004**, *37*, 326.
(5) (a) Qu, L. H.; Peng, X. G. *J. Am. Chem. Soc.* **2002**, *124*, 2049. (b) Sun, S. H.; Murray, C. B.; Weller, D.; Folks, L.; Moser, A. *Science* **2000**, *287*, 1989. (c) Chen, C. C.; Herhold, A. B.; Johnson, C. S.; Alivisatos, A. P. *Science* **1997**, *276*, 398. (d) Sun, S. H.; Zeng, H.; Robinson, D. B.; Raoux, S.; Rice, P. M.; Wang, S. X.; Li, G. X. *J. Am. Chem. Soc.* **2004**, *126*, 273.
(6) (a) Peng, X. G.; Manna, L.; Yang, W. D.; Wickham, J.; Scher, E.; Kadavanich, A.; Alivisatos, A. P. *Nature* **2000**, *404*, 59. (b) Hu, J. T.; Li, L. S.; Yang, W. D.; Manna, L.; Wang, L. W.; Alivisatos, A. P. *Science* **2001**, *292*, 2060. (c) Mikulec, F. V.; Kuno, M.; Bennati, M.; Hall, D. A.; Griffin, R. G.; Bawendi, M. G. *J. Am. Chem. Soc.* **2000**, *122*, 2532.
(7) (a) Manna, L.; Milliron, D. J.; Meisel, A.; Scher, E. C.; Alivisatos, A. P. *Nat. Mater.* **2003**, *2*, 382. (b) Milliron, D. J.; Hughes, S. M.; Cui, Y.; Manna, L.; Li, J. B.; Wang, L. W.; Alivisatos, A. P. *Nature* **2004**, *430*, 190.
(8) (a) Teng, X. W.; Yang, H. *Nano Lett.* **2005**, *5*, 885. (b) Lee, S. M.; Jun, Y. W.; Cho, S. N.; Cheon, J. *J. Am. Chem. Soc.* **2002**, *124*, 11244.
(9) Cui, Y.; Banin, U.; Bjork, M. T.; Alivisatos, A. P. *Nano Lett.* **2005**, *5*, 1519.
(10) de Mello, Donega, C.; Liljeroth, P.; Vanmaekelbergh, D. *Small* **2005**, *1*, 1152.
(11) (a) Peng, Z. A.; Peng, X. G. *J. Am. Chem. Soc.* **2001**, *123*, 1389. (b) Chen, Y. F.; Kim, M.; Lian, G.; Johnson, M. B.; Peng, X. G. *J. Am. Chem. Soc.* **2005**, *127*, 13331. (c) Song, Q.; Zhang, Z. J. *J. Am. Chem. Soc.* **2004**, *126*, 6164.
(12) Epifani, M.; Siciliano, P.; Gurlo, A.; Barsan, N.; Weimar, U. *J. Am. Chem. Soc.* **2004**, *126*, 4078.
(13) Lei, Z. B.; Ma, G. J.; Liu, M. Y.; You, W. S.; Yan, H. J.; Wu, G. P.; Takata, T.; Hara, M.; Domen, K.; Li, C. *J. Catal.* **2006**, *237*, 322.

10.1021/ic061999f CCC: $37.00
Published on Web 05/27/2007

semiconductor too.[14] Both cubic and hexagonal In_2O_3 are good n-type semiconductors with band gaps of 3.55−3.75 eV (which is close to that of GaN) and have been used widely as solar cells,[15] transparent conductors,[16] and sensors (viz., in detecting NO_2,[17] NH_3,[18] and DNA[19]). Up to now, $In(OH)_3$, InOOH, and In_2O_3 nanostructures, including 1D nanowires,[20] nanotubes[21] and nanorods,[22] quasi-monodisperse nanocrystals,[23] nanocubes,[24] hollow spheres,[14] and needlelike particles[25], have been synthesized through CVD,[20] the organic solution synthetic route, the hot-injection technique,[23a] a hydrothermal reaction,[24] a solvothermal reaction,[22b] or by sonohydrolysis,[25a] and so forth.

Recently, we have developed a novel, general, and convenient liquid−solid−solution (LSS) strategy in order to synthesize monodispersed nanocrystals.[26,27] On the basis of this technique, here, a systematic study of the controlled synthesis of indium hydroxides, oxyhydroxides, and the oxides series has been carried out. $In(OH)_3$ nanocubes, nanorods, and InOOH star-shaped multipods, irregular nanoparticles have been synthesized. The size, shape, and composition can be controlled by adjusting the alkali concentration and the solvent polarity. Cubic and hexagonal In_2O_3 can be obtained from $In(OH)_3$ and InOOH upon heating, respectively, while size and morphology can be maintained during this process. Gas sensors were fabricated by the as-prepared In_2O_3 and show high sensitivity for detection of ethanol vapor. Some preliminary investigations on the structural-based gas-sensing properties have been carried out. Compared to the nanocubes and nanorods, the multipod-based sensor shows the best responses.

Experimental Section

I. Chemicals. All of the the reagents were of analytical grade and used as received without any further purification. Deionized water was used throughout in the experiments. Indium nitrate ($In(NO)_3 \cdot 5H_2O$), sodium hydroxide (NaOH), ethanol (C_2H_5OH), oleic acid ($CH_3(CH_2)_7CH{=}CH(CH_2)_7COOH$), and cyclohexane ($C_6H_{12}$) were purchased from the Beijing Chemical Factory, China.

II. Synthesis. In a typical synthesis of $In(OH)_3$ nanocubes, 0.5 g NaOH was put into a Teflon-lined autoclave of 50 mL capacity and dissolved in deionized water (10 mL). Then, ethanol (8 mL), cyclohexane (8 mL), and oleic acid (3.5 mL) were introduced into the solution. After mixing for 5 min under stirring, $In(NO_3)_3 \cdot 5H_2O$ (0.2 g, 0.0005 M) was added to the emulsion. After stirring for 5 min, the autoclave was sealed and heated at 200 °C for 20 h. Then, the autoclave was allowed to cool to room temperature naturally. The resulting white suspensions were centrifuged for 5 min at 4500 rpm, and the bottom precipitates were thoroughly washed with ethanol and dried in air at 50 °C.

Similarly, $In(OH)_3$ nanorods were prepared by reducing the amount of cyclohexane from 8 mL to 2 mL.

For the synthesis of InOOH, the amount of NaOH was reduced from 0.5 to 0.2 g. For star-shaped InOOH multipods, the amount of ethanol was 8 mL and cyclohexane was 2 mL. For irregular nanoparticles, the amount of ethanol was 10 mL and no cyclohexane was introduced.

III. Redispersion. Product (0.03 g) was added into cyclohexane (10 mL). After sonicating for 5 min, they were centrifugated for 3 min at 4000 rpm. The supernatant containing suspended particles was then poured off and saved, and any precipitates were discarded.

IV. Transformation into In_2O_3. The redispersed colloidal nanocrystals were dropped on a silicon substrate and put in a furnace for 2 h in air. For $In(OH)_3$, the temperature was set at 300 °C; and for InOOH, it was set at 400 °C.

V. Characterization. The product phase was examined using X-ray diffraction (XRD) on a Bruker D8 Advance X-ray powder diffractometer with Cu Kα radiation ($\lambda = 1.5418$ Å). Size and morphology of nanocrystals were characterized by means of transmission electron microscopy (TEM, JEM 1200EX), high-resolution transmission electron microscopy (HRTEM, Tecnai G2 F20 S-Twin), and scanning electron microscopy (SEM, Sirion 200). The gas-sensing measurement system was fabricated by Hanwei Electronics Co. Ltd., Henan, PR China.

Results and Discussion

Synthetic Route and Characterization of $In(OH)_3$ and InOOH Nanocrystals. In our synthetic strategy, indium hydroxides and oxyhydroxides were obtained by the hydrolysis of In^{3+} in an aqueous solution. $In(NO_3)_3 \cdot 5H_2O$ was selected as the indium source. Sodium oleate was employed as the coordinating agent, which can react with In^{3+} and control the growth of $In(OH)_3$ or InOOH nuclei. On the basis of the LSS mechanism,[26] In^{3+} in the aqueous solution will first react with the excess sodium oleate, which leads to the formation of indium oleate. Then, at a designated temperature, indium oleate hydrolyzes at the liquid−solid or solution−solid interfaces. The in-situ-generated oleic acid will cover the surfaces of indium hydroxides or oxyhydroixdes and confine further product growth. Through this LSS

(14) Zhu, H. L.; Yao, K. H.; Zhang, H.; Yang, D. R. *J. Phys. Chem. B* **2005**, *109*, 20676.
(15) Katoh, R.; Furube, A.; Yoshihara, T.; Hara, K.; Fujihashi, G.; Takano, S.; Murata, S.; Arakawa, H.; Tachiya, M. *J. Phys. Chem. B* **2004**, *108*, 4818.
(16) (a) Gordon, R. G. *MRS Bull.* **2000**, *25*, 52. (b) Kim, H.; Horwitz, J. S.; Kushto, G. P.; Qadri, S. B.; Kafari, Z. H.; Chrisey, D. B. *Appl. Phys. Lett.* **2001**, *78*, 1050.
(17) (a) Zhang, D. H.; Liu, Z. Q.; Li, C.; Tang, T.; Liu, X. L.; Han, S.; Lei, B.; Zhou, C. W. *Nano Lett.* **2004**, *4*, 1919. (b) Pinna, N.; Neri, G.; Antonietti, M.; Niederberger, M. *Angew. Chem., Int. Ed.* **2004**, *43*, 4345. (c) Gurlo, A.; Barsan, N.; Weimar, U.; Ivanovskaya, M.; Taurino, A.; Siciliano, P. *Chem. Mater.* **2003**, *15*, 4377.
(18) Zhang, D. H.; Li, C.; Liu, X. L.; Han, S.; Tang, T.; Zhou, C. W. *Appl. Phys. Lett.* **200**3, *83*, 1845.
(19) Curreli, M.; Li, C.; Sun, Y. H.; Lei, B.; Gundersen, M. A.; Thompson, M. E.; Zhou, C. W. *J. Am. Chem. Soc.* **2005**, *127*, 6922.
(20) (a) Li, C.; Zhang, D. H.; Han, S.; Liu, X. L.; Tang, T.; Zhou, C. W. *Adv. Mater.* **2003**, *15*, 143. (b) Liang, C. H.; Meng, G. W.; Lei, Y.; Phillipp, F.; Zhang, L. D. *Adv. Mater.* **2001**, *13*, 1330.
(21) Fang, Y. P.; Wen, X. G.; Yang, S. H. *Angew. Chem., Int. Ed.* **2006**, *45*, 4655.
(22) (a) Lin, S. E.; Wei, W. C. J. *J. Am. Ceram. Soc.* **2006**, *89*, 527. (b) Yu, D. B.; Yu, S. H.; Zhang, S. Y.; Zuo, J.; Wang, D. B.; Qian, Y. T. *Adv. Funct. Mater.* **2003**, *13*, 497. (c) Zhang, X. H.; Xie, S. Y.; Ni, Z. M.; Zhang, X.; Jiang, Z. Y.; Xie, Z. X.; Huang, R. B.; Zheng, L. S. *Inorg. Chem. Commun.* **2003**, *6*, 1445.
(23) (a) Liu, Q. S.; Lu, W. G.; Ma, A. H.; Tang, J. K.; Lin, J.; Fang, J. Y. *J. Am. Chem. Soc.* **2005**, *127*, 5276. (b) Seo, W. S.; Jo, H. H.; Lee, K.; Park, J. T. *Adv. Mater.* **2003**, *15*, 795. (c) Lee, C. H.; Kim, M.; Kim, T.; Kim, A.; Paek, J.; Lee, J. W.; Choi, S. Y.; Kim, K.; Park, J. B.; Lee, K. *J. Am. Chem. Soc.* **2006**, *128*, 9326.
(24) (a) Tang, Q.; Zhou, W. J.; Zhang, W.; Ou, S. M.; Jiang, K.; Yu, W. C.; Qian, Y. T. *Gryst. Growth Des.* **2005**, *5*, 147. (b) Huang, J. H.; Gao, L. *Gryst. Growth Des.* **2006**, *6*, 1528.
(25) (a) Avivi, S.; Mastai, Y.; Gedanken, A. *Chem. Mater.* **2000**, *12*, 1229. (b) Perez-Maqueda, L. A.; Wang, L. F.; Matijecic, E. *Langmuir*, **1998**, *14*, 4397.
(26) Wang, X.; Zhuang, J.; Peng, Q.; Li, Y. D. *Nature* **2005**, *437*, 121.
(27) Ge, J. P.; Chen, W.; Liu, L. P.; Li, Y. D. *Chem.—Eur. J.* **2006**, *12*, 6552.

Table 1. The Reaction Conditions for Synthesizing $In(OH)_3$ and InOOH

water (mL)	ethanol (mL)	cyclohexane (mL)	NaOH (g)	product	morphology
10	8	8	0.5	$In(OH)_3$	nanocubes
10	8	2	0.5	$In(OH)_3$	nanorods
10	8	2	0.2	InOOH	star-shaped multipods
10	10	0	0.2	InOOH	irregular nanoparticles

synthetic technique, indium hydroxide and oxyhydroxide nanocrystals have been synthesized. By heating the products, cubic or hexagonal In_2O_3 nanocrystals will be obtained. To keep their morphologies, the temperature was selected near the phase-changing region, which is 300−400 °C.

In the experiment, we found that the alkali concentration and the solvent ratio (water, ethanol/cyclohexane) play important roles in the formation, nucleation, and growth of indium hydroxide or oxyhydroxide. Table 1 lists the reaction conditions for as-prepared indium hydroxides and oxyhydroxides with different structures and morphologies, respectively.

Figure 1 shows the XRD patterns of as-prepared samples. Parts a and b of Figure 1 are the patterns of $In(OH)_3$ nanocubes and nanorods, respectively, which show good agreement with the data reported in the literature (Figure 1c, JCPDS card number 76−1464). The (200) peak is particularly strong, which may come from the regular shape (cubic and rodlike) and ordered assembly of as-prepared $In(OH)_3$. Parts d and e of Figure 1 are the patterns of InOOH star-shaped multipods and irregular nanoparticles, respectively. They are consistent with reports in literature (Figure 1f, JCPDS card number 71−2283).

In the experiment, we found that the concentration of the alkali also has a major effect on the composition of the products. When there is more than 0.4 g of NaOH (10 mmol), pure $In(OH)_3$ will be obtained; and when there is less than 0.2 g NaOH (5 mmol), pure InOOH will be obtained instead. Simply, it can be considered that, at a higher alkali concentration, the products will be difficult to dehydrate and will contain more OH^-. However, too much NaOH is not good for synthesizing $In(OH)_3$. Although pure $In(OH)_3$ can be obtained at a very high alkali concentration, the hydrolyzing speed of the $In(NO)_3$ is too fast, which will lead the morphology of product out of control. In our synthetic process, it is found that 0.5 g NaOH is the best amount for $In(OH)_3$ synthesis. InOOH is usually considered as a metastable phase, which can only be synthesized under high-pressure conditions.[28] In our reaction system, the special environment (a closed system in which the solvent achieves a critical state) makes it easily obtainable.

Transmission electron microscopy (TEM) and high-resolution transmission electron microscopy (HRTEM) were employed to investigate the structures of the as-prepared samples. Figure 2 shows the TEM and HRTEM images of the $In(OH)_3$ nanocubes obtained with a high concentration

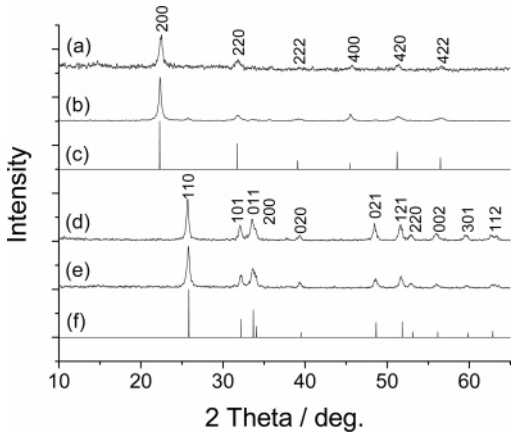

Figure 1. XRD patterns of as-prepared samples (a) $In(OH)_3$ nanocubes, (b) $In(OH)_3$ nanorods, (c) standard pattern of $In(OH)_3$ (JCPDS card number 76−1464), (d) star-shaped InOOH multipods, (e) InOOH irregular nanoparticles, and (g) standard pattern of InOOH (JCPDS card number 71−2283).

of cyclohexane. Figure 2a is an image of $In(OH)_3$ nanocubes with low magnification. Because the surface of the nanocrystals was capped with oleic acid, these cubes are well dispersed on the grid. It can be found that the length-to-width aspect ratios of most nanocrystals are less than 2, and the edge length of the cubes is about 12−17 nm. Becuase of the cubic morphology and the narrow size distribution, the cubes can self-assemble to a 2D pattern. The inset in Figure 2a shows the SAED pattern of a number of nanocubes, in which all of the reflections have been indexed and are consistent with the XRD result.

Figure 2b shows the low-magnification HRTEM image of nanocubes. Between the two neighboring nanocubes, there is a space of about 2.8 nm, which corresponds to the thickness of the double layer of oleic acid.[29] This phenomenon indicates that the interaction between the surfactants capped around nanocrystals plays an important role in the 2D pattern formation. Because of the low decomposition temperature (about 200 °C) of $In(OH)_3$, these as-prepared nanocubes can dehydrate during the HRTEM analysis process (under high-energy electron beam irradiation). By careful observation, there is a variety of brightness in the cubes, which indicates partial decomposition of the nanocubes. Figure 2c shows a typical HRTEM image of a partially decomposed $In(OH)_3$ nanocube. From the lattice fringes, it is found that the orthogonal and equivalent lattice fringes (indicated inside the arc) are typical symbols of cubic structure, and the interplane distances are about 0.29 nm, which can be indexed to the (220) planes of cubic $In(OH)_3$. This indicates that the growth of cubic $In(OH)_3$ nanocrystals were terminated at {100} planes, which were predicted to have the lowest surface energy. This result agrees with the XRD patterns (shown in Figure 1a), in which the (200) peak is especially strong. The lattice fringes outside the arc show differences compared to $In(OH)_3$ (inside the arc) in both interplane distances and angles. This indicates that most areas of the nanocube may have decomposed. Interestingly, the nanocube seems to have a hollow structure.

(28) Greenwood, N. N. *Chemistry of the Elements*; Greenwood, N. N., Earnshaw, A. E., Eds.; Pergamon Press: New York, 1984; p 278.

(29) Huo, Z. Y.; Chen, C.; Li, Y. D. *Chem. Commum.* **2006**, 3522.

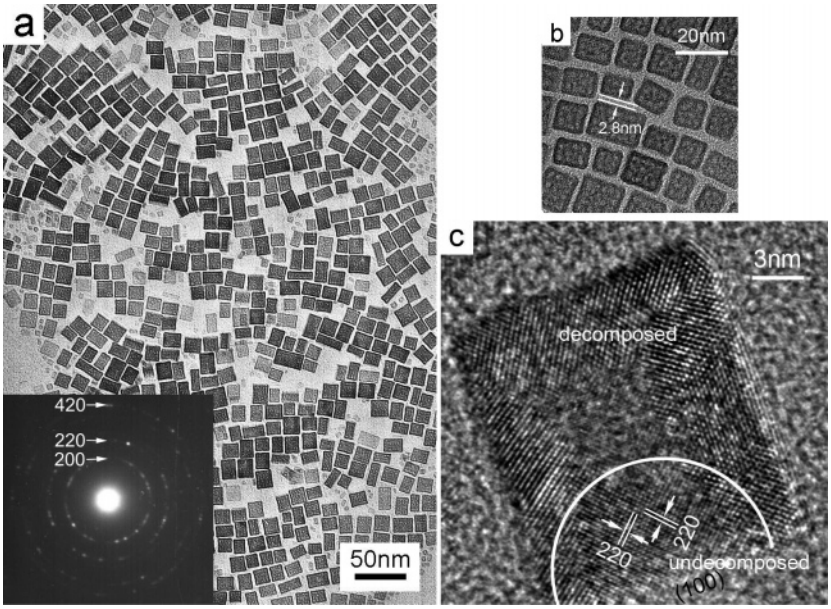

Figure 2. TEM images of $In(OH)_3$ nanocubes (a) low-magnification TEM image, and the inset is SAED pattern, (b) low-magnification HRTEM image, (c) HRTEM image of an individual partially decomposed $In(OH)_3$ nanocube, the interplane distances of orthogonal lattice fringes (inside the arc) are about 0.29 nm, which is corresponding to that of the (220) face of $In(OH)_3$.

From the HRTEM image (Figure 2c), it can also be found that the nanocubes are not single crystals but, rather, the assemblies of small crystals. Similar behavior has been observed by the Antonietti and Niderberger group and others.[30,31] During the growth process, large amounts of nuclei generated first and then grew up to primary nanoparticles. The primary nanoparticles are active, and some of them will orient and assemble into a larger nanocrystal. However, the assembly process may also bring some defects in the obtained crystals, which makes some parts of nanocrystals more easily decomposable. When the sample was under high-energy electron beam irradiation, based on the decomposition process, multicrystal-assembled and porous structures will form. This structure, which is also called a mesocrystal,[31] may create a new opportunity to facilitate the applications of indium hydroxide-based nanocrystals. This kind of mesocrystal is a special case of colloidal crystals, which can create materials with complex structures. Compared to single-crystal nanoparticles, porous mesocrystals have larger surface area, which may enhance properties such as catalysis and gas sensing. These kinds of self-alignment crystal assemblies of semiconductors may also bring new electronic and optical properties to materials.

Typical images of $In(OH)_3$ nanorods obtained with a low concentration of cyclohexane are shown in Figure 3. Figure 3a illustrates a low-magnification TEM image of the sample. More than 90% of the products are rodlike (length-to-width aspect ratios are more than 5) nanocrystallites, although there are still some cubic nanocrystals. The inset in Figure 3a shows the SAED pattern. According to the high-magnification TEM image (Figure 3b), it is found that these nanorods can also assemble regularly in a short range. They have a diameter of about 7−15 nm and a length of up to 50 nm. Like $In(OH)_3$ nanocubes, these nanorods can also decompose under electron beam irradiation. Figure 3c shows a typical HRTEM image of a partially decomposed nanorod, which is also a multicrystal assembly and has a multicavity hollow structure (indicated by an arrow). Figure 3d is a typical undecomposed $In(OH)_3$ nanorod. The interplane distance of lattice fringes is about 0.29 nm, which corresponds to that of the (220) face of $In(OH)_3$ and indicates these rods grow along the [100] direction.

The polarity of the solvent is another important factor in determining the structure and morphology of products. Cyclohexane is a nonpolar solvent, and the others (water and ethanol) in our experiments are all polar solvents. The polarity of the solvent can be adjusted by altering the amount of cyclohexane, which can further control the nucleation and growth of $In(OH)_3$. When a large amount of hexane (8 mL) was introduced, cubic nanocrystals, which have a high symmetry, were obtained. When the amount of cyclohexane was decreased to 2 mL, rodlike nanocrystals were produced instead of nanocubes. $In(OH)_3$ is an ionic compound, and the surface-electron and dipole−dipole interactions are important factors to the nanocrystal growth. As a result of the surface defects and the distribution of electric charge, nanocrystals usually have nonzero dipole moments.[32] In a higher polar solvent, the dipole moments are larger, so they have stronger dipole−dipole interactions between nanocrystals. The dipole−dipole interactions may cause the nanocrystals to favor growth in a particular direction. An increase in solvent polarity will lead nanocrystals to grow faster along a particular direction, resulting in rodlike nanocrystals. Oppositely, a low solvent polarity will form an equivalent

(30) Polleux, J.; Antonietti, M.; Niederberger, M. *J. Mater. Chem.* **2006**, *16*, 3969.
(31) (a) Colfen, H.; Antonietti, M. *Angew. Chem., Int. Ed.* **2005**, *44*, 5576. (b) Yu, S. H.; Colfen.; H.; Tauer, M.; Antonietti, M. *Nat. Mater.* **2005**, *4*, 51.
(32) Cho, K. S.; Talapin, D. V.; Gaschler, W.; Murray, C. B. *J. Am. Chem. Soc.* **2005**, *127*, 7140.

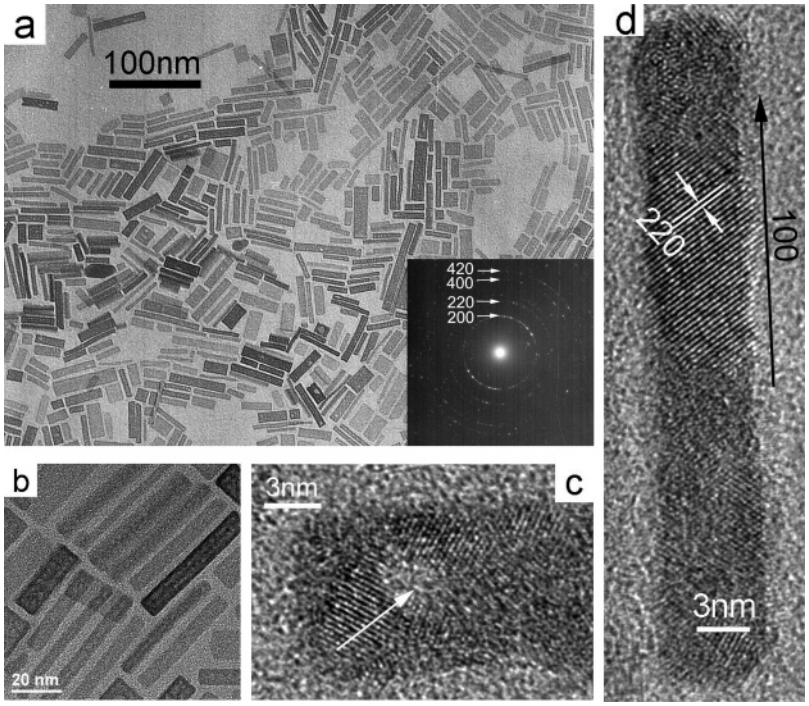

Figure 3. TEM images of $In(OH)_3$ nanorods (a) and (b) at different magnifications, the inset is the SAED pattern, (c) HRTEM image of a typical partially decomposed nanorod, with the hollow area marked with an arrow, and (d) HRTEM image of an individual undecomposed $In(OH)_3$ nanorod.

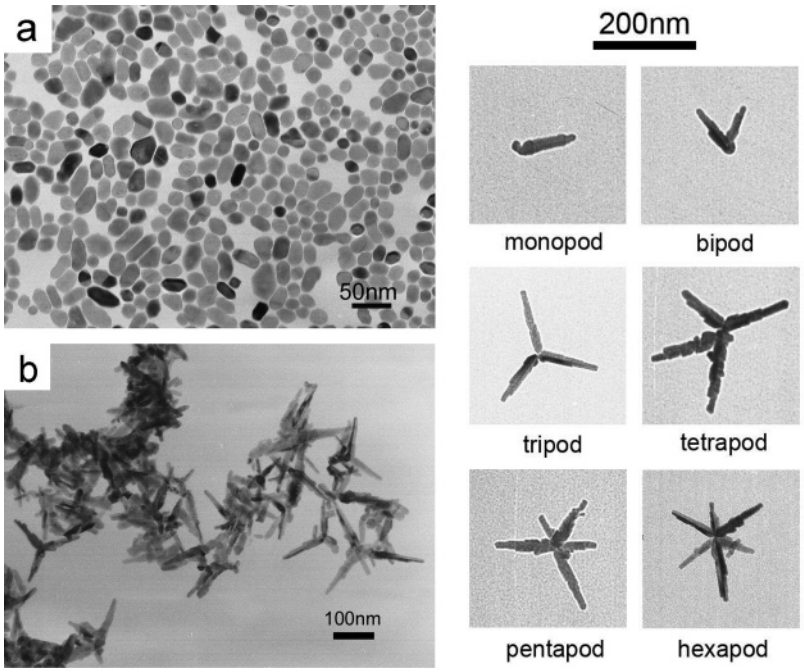

Figure 4. (a) TEM image of InOOH irregular nanoparticles, (b) TEM of InOOH multipods (over-head view), and (c) magnified TEM images of multipods from monopod to hexapod, respectively.

environment, which benefits the growth of nanocrystals with high symmetry.

Figure 4 illustrates TEM images of as-prepared InOOH. In Figure 4a are irregular InOOH nanoparticles obtained without introducing cyclohexane. They have an average diameter of about 20 nm. Parts b and c of Figure 4 show InOOH obtained with 2 mL cyclohexane, which has a star-shaped multipod structure. These nanocrystals have structures ranging from monopodal to hexapodal (Figure 4c), with the majority having a tripodal structure. The arms of these multipods have lengths of about 100 nm and widths of about 20 nm. In a typical tripodal structure, the lengths of three arms are nearly the same, and the angle between two arms is about 120°. Because the image is a 2D projection of a stereo 3D structure, the tripod may have a trigonal-pyramidal structure, and the three arms grow along different faces of a polyhedron core. The hexapod can also be considered as two coupled tripods, and three more arms grow along opposition directions of the tripod (a distorted octahedral structure). The other multipods may be defective tripods or hexapods. Under

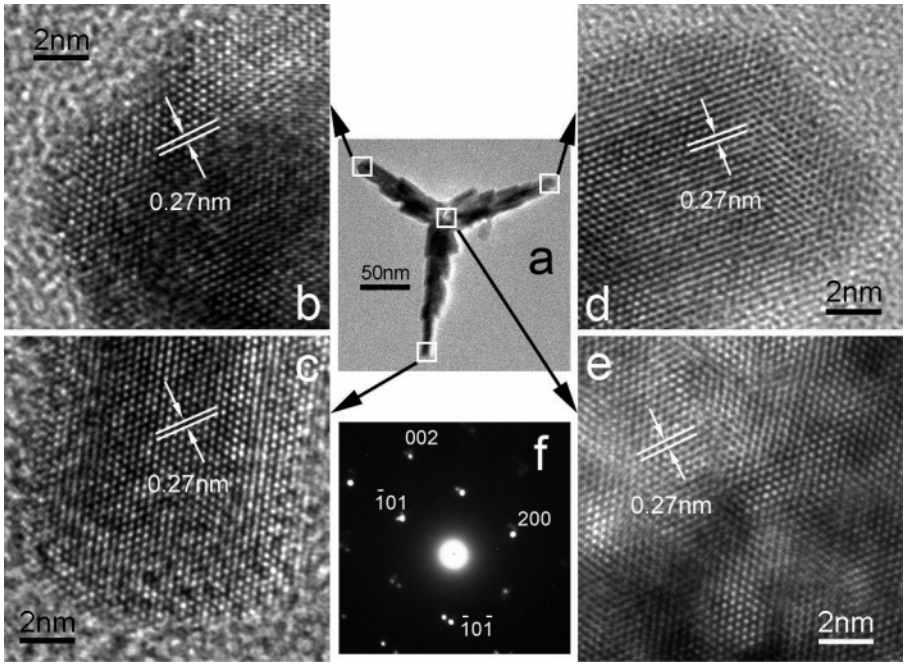

Figure 5. HRTEM images and SAED pattern of a typical tripod (a) over-head view, (b), (c), and (d) three arms at high magnification, (e) core at high magnification, and (f) SAED pattern of the whole tripod.

careful observations, these multipods seem to have hierarchical structures. Each of the arms has secondary growth directions, which may form fractal structures.

Figure 5 shows the HRTEM images of a typical tripod nanocrystal. Figure 5f is the SAED pattern of the whole tripod, which indicates that the tripod nanocrystal is a single crystal. Four HRTEM images (parts b−e of Figure 5, three arms and the center, respectively) show good crystallinity of the tripod, and the similarity of lattice fringes (they have the same interplane distance of 0.27 nm and the same direction) also indicate the tripod is a single crystal. Unlike other multipod structures reported in the literature (they usually have a cubic crystal cell, and the arms grow along the equal crystal faces),[7,8] InOOH has an orthorhombic crystal cell, which has a relatively lower symmetry than cubic ones. On the basis of the SAED pattern (Figure 5f), we found that the three arms are grow along [200], [$\bar{1}$01], and [$\bar{1}0\bar{1}$] faces, respectively. Although they are not in the same direction, the interplanar spacing of these crystal faces are similar (from the XRD result, it is known that the interplanar spacing of the (200) face is 2.63 Å and that of the (101) face is 2.77 Å), so the three arms have near-packing speeds, which causes the lengths of the arms to be similar. This phenomenon indicates that not only the cubic-phase compounds with equal crystal faces but also the others with near-interplanar spacing can form multipods. This novel structure combines 1D structures to a 3D structure, which may have excellent electronic properties and potential applications in nanotechniques, such as fabricating a multiterminal device, and so forth.

The generation of multipods is usually considered the aggregation of crystalline subunits.[31] At the early stage of reactions, small nanocrystals (crystalline subunits) are generated and temporary stabilized by oleic acid. Then, the orientational alignments make the crystalline subunits aggregate and form mesocrystals. The oleic acid inside the mesocrystals can be removed and the mesocrystal will fuse as a single crystal.[31] For InOOH, the crystal faces of [200], [$\bar{1}$01], and [$\bar{1}0\bar{1}$] have similar interplanar spacing, where the crystalline subunits may orientationally align along these faces from one crystal core and finally form a multipod structure. The secondary growth and formation of hierarchical structures on the multipods may also come from this aggregation and fuse process.

Transformation into In_2O_3. Like other metal hydroxides, indium hydroxide and oxyhydroxide can dehydrate to form indium oxides upon heating.[12,33] In_2O_3 has two types of crystal structures (cubic and hexagonal), and in both structures, In^{3+} ions are six-coordinated and O^{2-} ions are four-coordinated. However, there are obvious differences. Cubic In_2O_3 (space group *Ia*3) can be described as an oxygen-deficient fluorite structure with twice the unit-cell edge of the corresponding fluorite cell and one-quarter of the anions missing in an ordered way. In hexagonal In_2O_3 (space group *R*3*c*), the In^{3+} ions are distributed in an ordered fashion over two-thirds of the octahedral sites within a framework of hexagonally close-packed O^{2-} ions.[12,28] Cubic $In(OH)_3$, with a space group of *Im*3, has a simple distorted ReO_3-type structure with multiple hydrogen bonds. Orthorhombic InOOH, with a space group of *Pnnm*, has a deformed rutile structure rather than the layer lattice structure of AlOOH and GaOOH. In our experiments, cubic $In(OH)_3$ can transform into cubic In_2O_3 and orthorhombic InOOH can transform into hexagonal In_2O_3 upon heating. To keep the original morphologies from $In(OH)_3$ and InOOH possible, the heating

(33) (a) Singh, V. N.; Mehta, B. R. *J. Nanosci. Nanotechnol.* **2005**, *5*, 431. (b) Zhu, H. L.; Wang, N. Y.; Wang, L. N.; Yao, K. H.; Shen, X. F. *Inorg. Mater.* **2005**, *41*, 702.

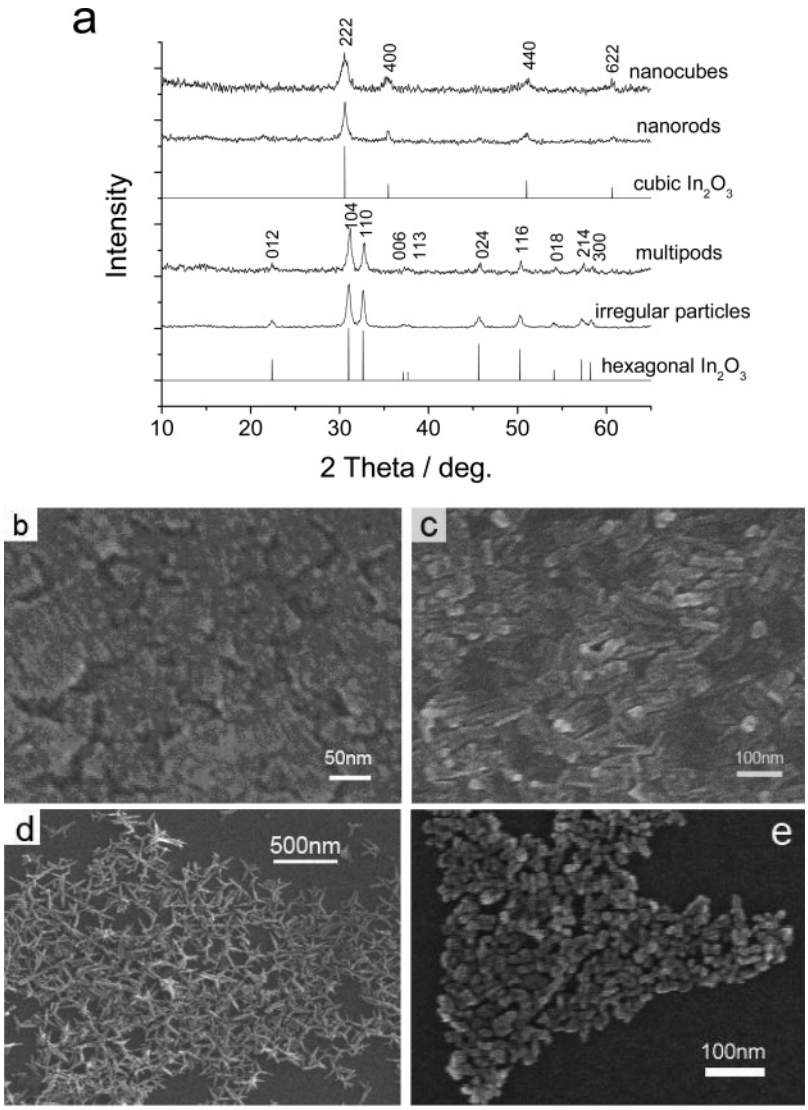

Figure 6. XRD patterns (a) and SEM images (b) cubic In_2O_3 from $In(OH)_3$ nanocubes, (c) cubic In_2O_3 from $In(OH)_3$ nanorods, (d) hexagonal In_2O_3 from InOOH multipods, and (e) hexagonal In_2O_3 from InOOH irregular nanoparticles.

temperatures were selected at a little above of the phase-changing temperature (300 °C for $In(OH)_3$ and 400 °C for InOOH).

Figure 6 shows the XRD patterns of as-prepared In_2O_3 nanocrystals, which indicate that all of these samples are purely cubic or hexagonal In_2O_3. They are all in good agreement with the reports in the literature (cubic In_2O_3, JCPDS card number 76−0152; hexagonal In_2O_3, JCPDS card number 22−0336). The SEM images (parts b−e of Figure 6) indicate that all of these samples can keep the morphologies and sizes to a certain extent after annealing.

Gas-Sensing Properties for Ethanol Vapor. In recent years, many gas sensors based on n-type semiconductors have been researched. In_2O_3, known as a wide-band-gap n-type semiconductor, shows outstanding sensitivity for detecting NO_2,[19] NH_3,[20] O_3,[19c] and so forth. Herein, gas sensors were fabricated on the basis of the as-prepared cubic or hexagonal In_2O_3 with different morphologies (Figure 6) and show high sensitivities to ethanol vapor. Some preliminary investigations on structural-based gas-sensing properties have been carried out.

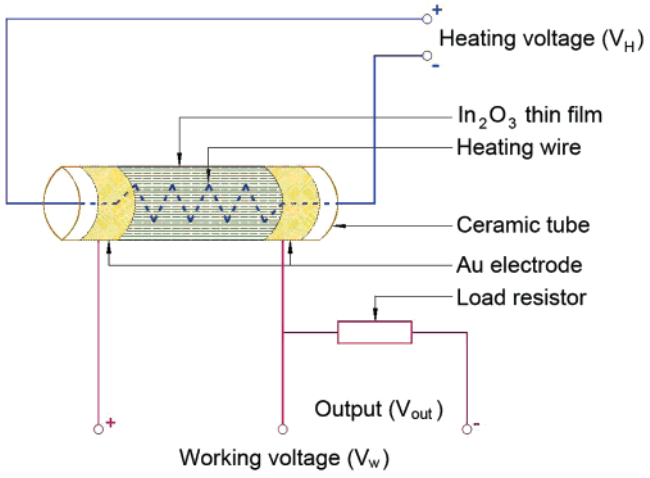

Figure 7. Schematic illustration of the sensor system.

Figure 7 shows the schematic diagram of the sensor system. First, homogeneous $In(OH)_3$ or InOOH colloidal supernatant was dropped onto a ceramic tube, on which a pair of Au electrodes were previous printed. After the solvent

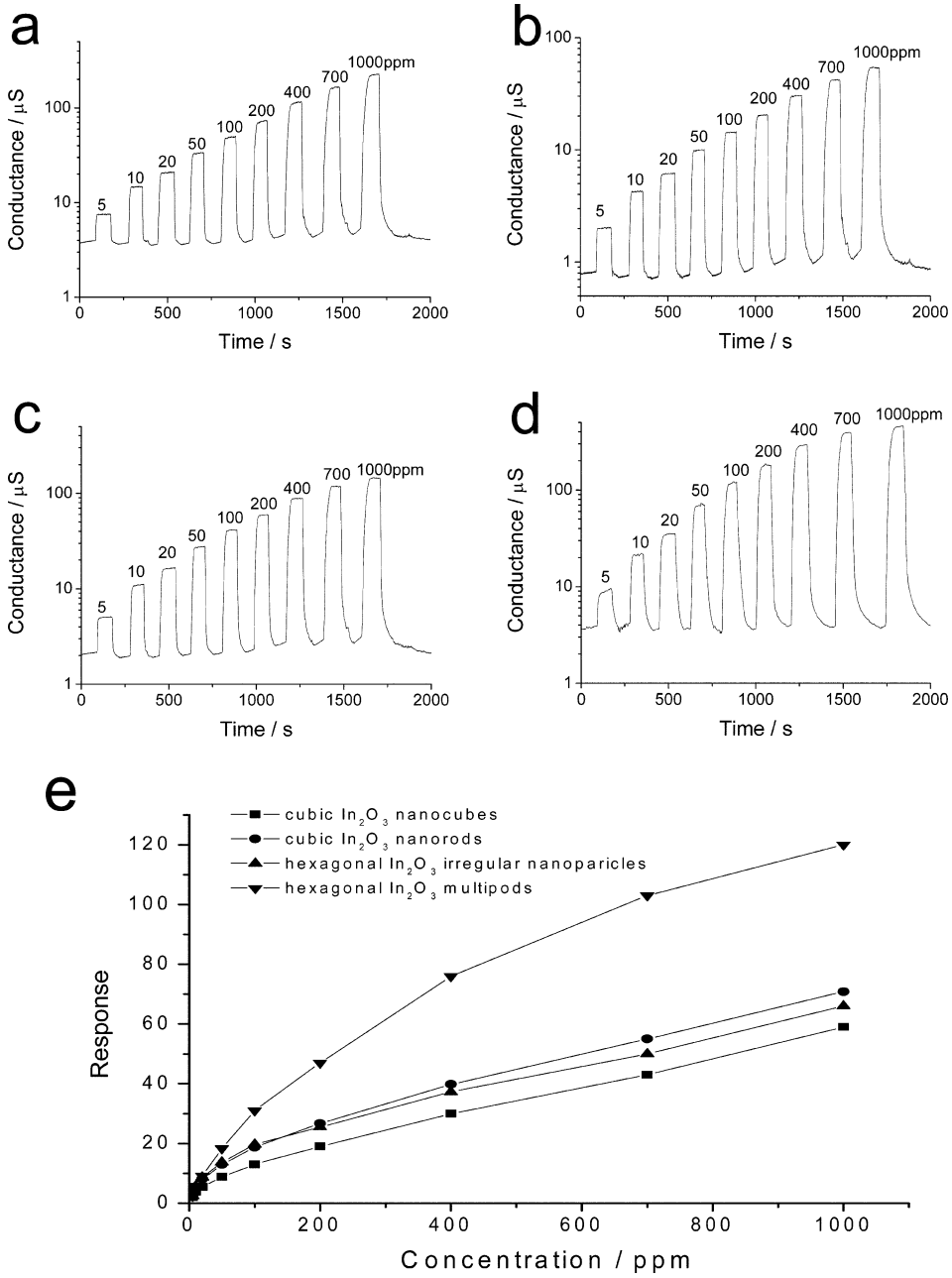

Figure 8. Typical response curves on cycling between increasing concentration (5−1000 ppm) of ethanol and ambient air (a) cubic In_2O_3 nanocubes, (b) cubic nanorods, (c) hexagonal In_2O_3 irregular nanoparticles, (d) hexagonal In_2O_3 multipods, and (f) the response ($S = G_g/G_a$) versus ethanol concentration.

evaporated, the colloidal crystals will assemble themselves and form a thin film. Then, the ceramic tube was annealed at 300 or 400 °C for 2 h. This process will make $In(OH)_3$ or InOOH transform into cubic In_2O_3 or hexagonal In_2O_3, and the device is stabilized in the meantime. Finally, a Ni−Cr heating wire was inserted into the tube, and the gas sensor was fabricated. The working temperature can be controlled by adjusting the heating voltage (V_H). In the test process, a load resistor was serialized and a working voltage (V_w) at 10 V was applied to this system. By monitoring the load resistor voltage (V_{out}), the response of the sensor in air or in a test gas can be measured. From Ohm's law, the resistance or conductance of the sensor can be worked out.

Before sensitivity measurement, the samples were maintained at 350 °C until the stabilization of the base line. Our gas-sensing measurements were made in a static system, and in each cycle, an appropriate amount of ethanol was injected into the testing chamber. After each measurement, the sensor was exposed to ambient air by opening the chamber and vent fan.

Both cubic and hexagonal In_2O_3 are n-type semiconductors, in which the electrons are considered as the majority carriers. The conductivity of In_2O_3 can be increased by the contributing free electrons from guest molecules. Ethanol, known as a reducing compound, can provide electrons when oxidated. The sensing mechanism can be considered as the following: First, the oxygen molecule in the air was absorbed onto the surface of the In_2O_3 thin film. It will form O_2^-, O^-, or O^{2-} and create a space-charge region near the surface of the film. Second, ethanol was absorbed and reacted with

the ionic oxygen species. Then, ethanol was oxidated and electrons were injected into the In_2O_3 film, which lead to an increase in conductance.

Parts a−d of Figure 8 plot the changes in sensor conductance as a function of time when the sensors are working at 350 °C. Nine cycles were successively recorded, corresponding to nine different ethanol concentrations ranging from 5 to 1000 ppm, respectively. The conductance undergoes a drastic rise upon the injection of ethanol and drops to its initial value after ethanol was released. These sensors show a high and quick response (response time is less than 10 s). The recovery time is about 15 s, which is defined as the time necessary for the sample to return to 10% above the original conductance in air after the test gas has been released.

The response of the sensor correlates to the concentration of the test gas and the structure and morphology of In_2O_3 (Figure 8e). The response is defined as $S = G_g/G_a$, where G_g and G_a are the conductance of the sensor in test gas and in air, respectively. The as-prepared sensors have better responses than that reported in the literature.[34] The lowest detection limit is down to 1 ppm. We found that the response depends on the phases and morphologies of In_2O_3. First, the sensor based on hexagonal In_2O_3 is more sensitive than that based on cubic In_2O_3. Hexagonal In_2O_3 is in a metastable phase, which is more active than the stable-phase cubic In_2O_3. During the test process, it is easier to absorb the target gas molecules, so it gets a higher response. Second, the 1D materials may enhance the response.[35] 1D material, which is considered as the smallest-dimension structures that can be used for efficient transport of electrons,[36] is more beneficial for transporting electrons than nanoparticles. In our experiments, sensors based on cubic In_2O_3 nanorods have a better response than those based on cubic In_2O_3 nanocubes, and sensors based on hexagonal In_2O_3 multipods have a better response than those based on hexagonal In_2O_3 nanoparticles. The multipod-based sensor (which can be considered as an advanced structure of 1D nanorods) shows a very high response.

Stability tests were finally performed on these sensors. After hundreds of cycling tests, the sensors still have good sensitivity and fast response and recovery times. This result shows both the sensitivity and the reproducibility of these sensors, and they can be applied in human breath.

Conclusion

In conclusion, highly sensitive and stable ethanol sensors based on In_2O_3 nanocrystals have been successfully developed. Both cubic and hexagonal In_2O_3 can be obtained by dehydration of $In(OH)_3$ or InOOH, which can be synthesized by a simple solvent method. The phases ($In(OH)_3$ and InOOH) and the morphologies (nanocubes, nanorods, multipods, and irregular nanoparticles) of the products can be controlled by adjusting the amount of NaOH and cyclohexane. Some preliminary investigations on the structural-based gas-sensing properties have been carried out. They indicates that the sensor based on hexagonal multipods has the best response to ethanol vapor. This work can enrich the comprehension of the structural−functional relationship of these sensors and can direct us to develop higher-quality gas sensors.

Acknowledgment. This work was supported by NSFC (Grants 20401010 and 50372030) and the State Key Project of Fundamental Research (Grant 2006CB0N0608).

IC061999F

(34) Chu, X. F.; Wang, C. H.; Jiang, D. L.; Zheng, C. M. *Chem. Phys. Lett.* **2004**, *399*, 461.
(35) Liu, J. F.; Wang, X.; Peng, Q.; Li, Y. D. *Adv. Mater.* **2005**, *17*, 764.
(36) Hu, J. T.; Odom, T. W.; Lieber, C. M. *Acc. Chem. Res.* **1999**, *32*, 435.